Annals of Biomedical Engineering, Vol. 36, No. 10, October 2008 (© 2008) pp. 1649–1658
DOI: 10.1007/s10439-008-9539-3

Quantitative Panoramic Imaging of Epicardial Electrical Activity

QING LOU, CRYSTAL M. RIPPLINGER, PHILIP V. BAYLY, and IGOR R. EFIMOV

Department of Biomedical Engineering, Washington University in St. Louis, One Brookings Drive, Campus Box 1097, St. Louis, MO 63130-4899, USA

(*Received 7 April 2008; accepted 14 July 2008*)

Abstract—Fluorescent imaging with voltage- and/or calcium-sensitive dyes has revolutionized cardiac physiology research. Here we present improved panoramic imaging for optically mapping electrical activity from the entire epicardium of the Langendorff-perfused rabbit heart. Combined with reconstruction of the 3D heart surface, the functional data can be conveniently visualized on the realistic heart geometry. Methods to quantify the panoramic data set are introduced by first describing a simple approach to mesh the heart in regular grid form. The regular grid mesh provides substrate for easy translation of previously available non-linear dynamics methods for 2D array data. It also simplifies the unwrapping of curved three-dimensional surface to 2D surface for global epicardial visualization of the functional data. The translated quantification methods include activation maps (isochrones), phase maps, phase singularity, and electric stimulus-induced virtual electrode polarization (VEP) maps. We also adapt a method to calculate the conduction velocities on the global epicardial surface by taking the curvature of the heart surface into account.

Keywords—Panoramic fluorescent imaging, Optical mapping, Action potential, Mesh, Unwrapping, Conduction velocity.

INTRODUCTION

Transmembrane potential on the epicardial surface of the heart can be recorded optically.[11] To maximize the field of view, panoramic optical imaging was introduced by Lin and Wikswo[10] to map the entire ventricular epicardium from three different angles around the heart. Later, more efforts were devoted to this novel imaging methodology. Bray *et al.*[2] proposed to reconstruct the heart geometry and texture map the optical signal onto the geometric surface for better visualization. Kay *et al.*[9] implemented panoramic optical mapping on swine hearts, and Rogers *et al.*[14,15] applied this technology in the research of ventricular fibrillation. More recently, our group[13] developed a panoramic imaging system using three photo-diode arrays (PDAs, Hamamatsu) with high temporal resolution for research on mechanisms of cardiac defibrillation.

While panoramic imaging systems are being improved, the data analysis methods designed for panoramic data sets are still limited. One reason is that the available analysis tools do not easily lend themselves to the unstructured triangular mesh of the heart surface geometry. In this study, we employed a way to mesh the heart surface for translation of some common 2D analysis methods. Additionally, conduction velocity vector fields were estimated from the panoramic data set for the first time.

METHODS

Optical Mapping Experiments

The panoramic optical mapping system and Langendorff-perfused rabbit heart have been described previously.[13] Briefly, three photo-diode arrays were spaced 120° apart and faced towards the heart in the perfusion chamber. Light-emitting diode arrays were used as excitation light source for the voltage-sensitive dye. This system provides high temporal resolution (5000 frames/s) and sufficient spatial resolution (1.72 mm without interpolation). The excitation–contraction uncoupler blebbistatin[8] was used to suppress motion artifacts during optical recording. Thirty-six images of the heart were taken every 10° as the heart was rotated a full 360° at the end of the experiments for geometric reconstruction. Optical signals were registered with and texture-mapped onto the surface of the reconstructed geometry.

Geometry Reconstruction and Registration

The geometry of the rabbit heart was reconstructed through 36 digital images of the heart using

Address correspondence to Igor R. Efimov, Department of Biomedical Engineering, Washington University in St. Louis, One Brookings Drive, Campus Box 1097, St. Louis, MO 63130-4899, USA. Electronic mail: igor@wustl.edu

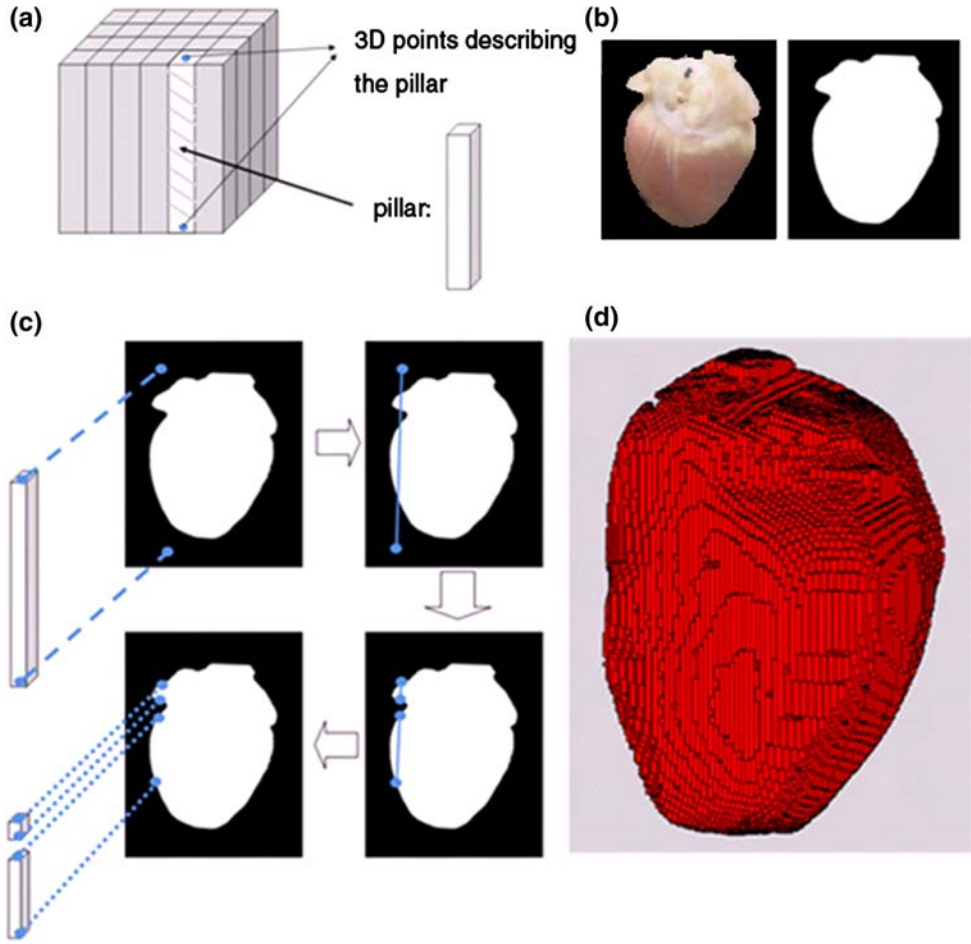

FIGURE 1. Reconstruction of heart geometry. (a) Pillars used as the building block for the geometry. (b) Digital image of the heart and silhouette image. (c) Refinement of the pillars using the silhouette image. First, the two end points of pillars were projected onto the images. The projections were then connected by a line which might intersect with the contour of the heart. The portions outside the contour were cropped off, and the corresponding part of the pillar was also cropped off. (d) The final reconstructed geometry of one heart.

Niem's method.[12] The procedures are illustrated in Fig. 1. A volume cube composed of pillar elements (Fig. 1a) was used as the first crude model of the heart for further refinement. The individual pillar was then projected consecutively into the digital images and tested for intersections with the object silhouettes (Fig. 1c). The part whose projection was outside the object silhouettes was carved off. By refining the volume cube with all the silhouettes in digital images, the geometry of the heart is reconstructed with sufficient details (Fig. 1d).

The registration of the signal with the geometric surface is accomplished by first projecting the reconstructed geometry onto the image plane of every PDA and then matching the projection with region of the heart "seen" by every PDA. Before each optical mapping study, a frosted glass was placed in the same location of image plane of every PDA and a digital image of the frosted glass was acquired. From these images the heart region for optical mapping from individual PDA was determined. Good registration is achieved when the projection (red dots in Fig. 2) perfectly matches the heart regions in the image plane of PDAs.

Unwrapping Heart Surface into 2D Map

Taking an approach similar to those used in cartography, the surface of the heart was "unwrapped" into a 2D flat map. This allows (1) global visualization of the data in a flat plane and (2) the direct utilization of well-established 2D analysis methods, such as isochronal mapping, estimation of conduction velocity vectors, and phase mapping.

The starting point of the unwrapping procedure is the identification of a large number of points (Fig. 3a) lying on the surface of the heart geometry; the coordinates of these points are obtained from geometric

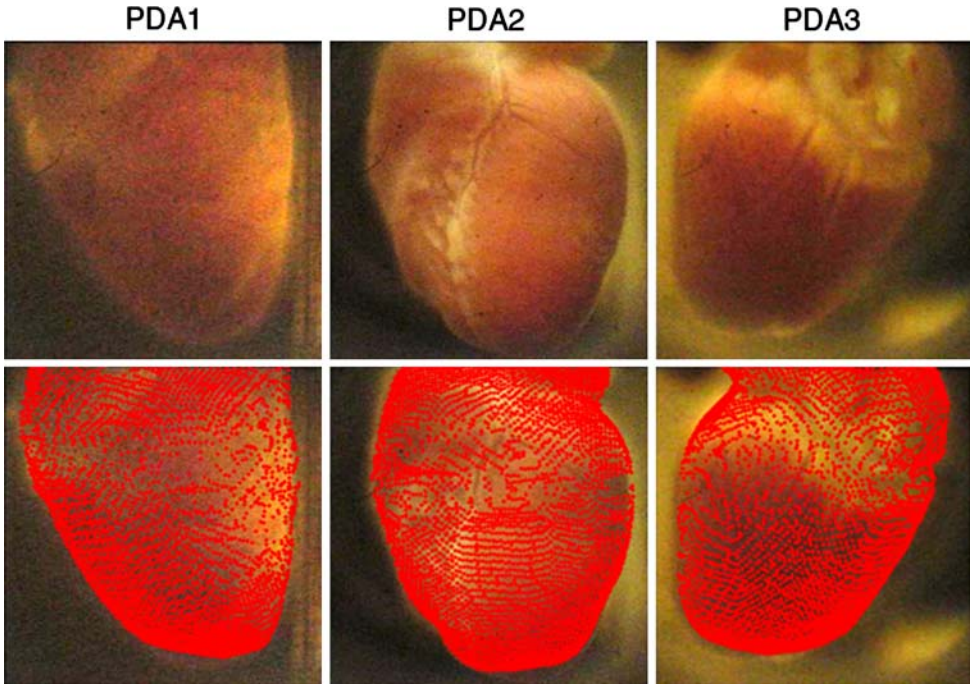

FIGURE 2. Registration of the recorded fluorescent signal with the reconstructed geometric surface. The images in the first row are digital images of the heart at the image plane of the PDAs. Red dots in second-row images are projections of the surface points of reconstructed geometry of the heart. Good registrations were reached when the shape of projections match and overlap the heart in the digital images.

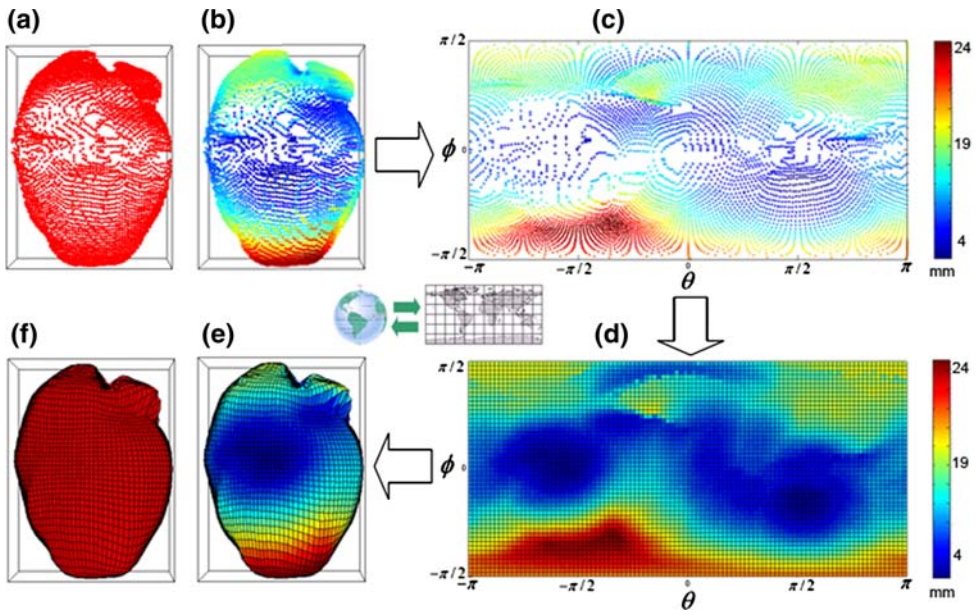

FIGURE 3. Meshing the heart surface. (a) Surface points obtained from geometric 3D reconstruction from multiple views. (b) Surface points coded with color which represents the distance to the geometric center of the heart. (c) Surface points unwrapped onto the (θ, φ) plane. (d) Linear interpolation of surface points into an evenly spaced (θ, φ) grid. (e) Meshed surface wrapped from interpolated grid. (f) Completed meshed surface.

reconstruction described in the previous section. The geometrical center of the heart is found by averaging the coordinates of all the heart surface points. Then the "longitude and latitude" of each point are calculated by transforming the Cartesian coordinates (x, y, z) to spherical coordinates (θ, φ, $\boldsymbol{r}$), where θ, φ are the

counterparts of longitude and latitude in the case of earth, and $\boldsymbol{r}$ is the distance between that point and the geometric center of the heart. The magnitude of $\boldsymbol{r}$ is represented by color in Fig. 3b. By redrawing every point in the θ–φ plane, we unwrap the heart surface into a two-dimensional "map." Again, the color of each point in Fig. 3c represents the magnitude of $\boldsymbol{r}$.

We then define an evenly spaced (θ, φ) grid, and interpolate $\boldsymbol{r}$ on this grid (Fig. 3d). Each grid element corresponds to a specific (θ, φ) pair. This procedure creates a 2D-grid representation of the heart surface which is compatible with many available data analysis tools. By connecting points with the same θ, and also points with the same φ in 3D space, we can generate a mesh (Fig. 3e, f) with lines mimicking the longitudes and latitudes in the Earth globe.

The resultant (θ, φ) plane is the 2D representation of the originally curved and topologically closed 3D surface. While it is a distorted representation of the curved heart surface, it provides an alternative way to visualize the epicardial activation, especially for global visualization without the necessity of rotating the heart. More importantly, it transforms the data structure into grid form so that common 2D analysis methods can be easily applied. Furthermore, if correlation between electrical activity and anatomical features is essential, we can also texture-map the anatomy onto the (θ, φ) plane.

Translate Data Analysis Methods

A variety of techniques to visualize and analyze the data were implemented, including maps of transmembrane voltage (V), dV/dt, phase, phase singularities, activation times, conduction velocity, and electric stimulus-induced virtual electrode polarization (VEP). Fluorescent signals were recorded from the PDAs. The signals were first normalized and then interpolated before being texture-mapped onto the surface.

Phase map is a unique tool for arrhythmic activity. It is based on phase plane analysis and facilitates visualization of wave fronts and wave breaks. Phase can be obtained using the method proposed by Bray and Wikswo.[3] Briefly, the phase $\psi(\theta, \varphi, t)$ is obtained by

$$\psi(\theta, \varphi, t) = \arctan \frac{V'(\theta, \varphi, t)}{H[V'(\theta, \varphi, t)]},$$

where $V'(\theta, \varphi, t)$ is the transmembrane voltage processed by the proper orthogonal decomposition, and $H[V'(\theta, \varphi, t)]$ is the Hilbert transform of $V'(\theta, \varphi, t)$ and represents a signal with a $\pi/2$ phase lag relative to $V'(\theta, \varphi, t)$.

Rotors or wave breaks during cardiac fibrillation correspond to the phase singularities in the phase map. The calculation of phase singularity was implemented based on the method described by Bray and Wikswo.[4] Briefly, the gradient of phase is first calculated along two dimensions of the θ–φ grid,

$$\nabla\psi_\theta[m, n] = \psi[m + 1, n] - \psi[m, n];$$
$$\nabla\psi_\varphi[m, n] = \psi[m, n + 1] - \psi[m, n].$$

Topological charge is then calculated using convolution between the gradients and 3×3 kernel which mimic the line integral of phase gradients along a closed curve surrounding a point. That is, $\nabla\psi_\theta \otimes \nabla_\theta + \nabla\psi_\varphi \otimes \nabla_\varphi$ where

$$\nabla_\theta = \begin{bmatrix} 0 & 0 & 0 \\ -1 & 0 & 1 \\ -1 & 0 & 1 \end{bmatrix}, \quad \nabla_\varphi = \begin{bmatrix} 0 & 1 & 1 \\ 0 & 0 & 0 \\ 0 & -1 & -1 \end{bmatrix}.$$

A point is recognized as a phase singularity if its topological charge is 2π or -2π.

Activation time was obtained using $(dV(\theta, \varphi, t)/dt)_{\max}$, from which the isochrones were generated.

All the methods described in this section can be first implemented in the (θ, φ) plane, and then wrapped back onto the 3D heart surface. It should be noted that we cannot directly apply this procedure to calculate the conduction velocity because distance is distorted in the (θ, φ) plane.

Conduction Velocity on the 3D Surface

Conduction velocity is an important parameter in determining the heart's susceptibility to arrhythmia. With the knowledge of the epicardial geometry, we are able to quantify conduction velocity on the whole heart surface.

One approach to calculate the conduction velocity in a 2D (x–y) plane has been proposed by Bayly *et al.*[1] Since the heart surface is essentially three dimensional, this method cannot be directly applied. We adapted this method and extended its usage in our panoramic data set. First, we define the activation time t as a function of θ and φ like $t(\theta, \varphi) = a\theta^2 + b\varphi^2 + c\theta\varphi + d\theta + e\varphi + f$, where θ and φ are spherical coordinates and has been calculated when we mesh the heart. Coefficients $a, b, \ldots, f$ are obtained by polynomial fitting using (t, θ, φ) in the pre-defined time and space windows. $\partial t/\partial\theta$ and $\partial t/\partial\varphi$ can then be calculated. The gradient of t is determined using

$$\nabla t = \frac{1}{r \sin\varphi}\hat{\theta}\frac{\partial t}{\partial\theta} + \frac{1}{r}\hat{\varphi}\frac{\partial t}{\partial\varphi} + \hat{r}\frac{\partial t}{\partial r}.$$

Since ∇t is zero along the direction normal to the surface, its projection on the direction normal to the surface should be equal to zero, that is,

$$\left(\frac{1}{r\sin\varphi}\hat{\theta}\frac{\partial t}{\partial\theta}+\frac{1}{r}\hat{\varphi}\frac{\partial t}{\partial\varphi}+\hat{r}\frac{\partial t}{\partial r}\right)\cdot\hat{e}_n=0 \qquad (1)$$

where $\hat{e}_n$ is the unit vector normal to the surface, and $\hat{\theta}$, $\hat{\varphi}$, and $\hat{r}$ are unit vectors in spherical coordinates. Since we know $\partial t/\partial\theta$ and $\partial t/\partial\varphi$, we can get $\partial t/\partial r$ by solving Eq. (1).

We then define two orthogonal axes, x and y, which are tangent to the surface; and calculate $\partial t/\partial x$ and $\partial t/\partial y$ by $\frac{\partial t}{\partial r}\frac{\partial r}{\partial x}$ and $\frac{\partial t}{\partial r}\frac{\partial r}{\partial y}$. $\partial t/\partial x$ and $\partial t/\partial y$ fully represent ∇t because ∇t is tangent to the surface. Finally, we can calculate the conduction velocity (CV) using

$$CV=\left[\frac{dx}{dt},\frac{dy}{dt}\right]=\left[\frac{t_x}{t_x^2+t_y^2},\frac{t_y}{t_x^2+t_y^2}\right],$$

where $t_x=\partial t/\partial x$ and $t_y=\partial t/\partial y$.

Simulations were performed to test the accuracy of this method on a meshed sphere which mimics the geometry of the heart. The mesh density of the sphere is set to be close to that of the reconstructed heart surface. A propagating wave is initiated from one surface point of the sphere, and radially propagates out on the surface at constant speed (Fig. 4a). The propagating wave with square cross sections was generated by the function $f(x,y,z,t)=sign(\sin(wt-k_r\boldsymbol{r}))$, where $\boldsymbol{r}$ is the surface distance away from the wave initiation site. The surface distance is the shortest distance between two points on the surface. The exact speed of propagation is w/k_r. The performance of this method was tested by calculating the deviation of the estimated from the exact propagation speed.

RESULTS

Function Together with Anatomy

Figure 5 shows the unwrapped anatomy, transmembrane voltage (V), dV/dt, phase map, and phase singularity in the (θ, φ) plane. Figure 5a is the anatomy map, which is obtained by first texture mapping the digital images of anatomy onto the reconstructed geometric surface and then unwrapping it into a flat plane. This unwrapped anatomy provides a unique way to correlate the functional data to the anatomy. Figure 5b is a snapshot of transmembrane voltage 230 ms after initiation of ventricular fibrillation. The value is normalized into −85 to 15 mV from the recorded fluorescent signal. Figure 5c is a snapshot of normalized dV/dt, where the largest values correspond to the wave fronts. Figure 5d is the phase map, with phase zero corresponding to the wave front. Figure 5e shows the distribution of phase singularities. Blue dots are the rotors of clockwise rotation of wavefront, while red dots are the rotors of counterclockwise rotation.

While the unwrapped view provides a global sense of wave propagation on the epicardium, data visualization on the reconstructed heart geometry provide an undistorted image of the electrical activation. It also allows for easy registration with the anatomy in the digital images at different angles. Figure 6 includes all the data presentations on the reconstructed geometry.

By mapping the whole ventricle, we are able to globally track the positions of phase singularities, which reveal the dynamics of the ventricular arrhythmia. The first image of Fig. 7 shows the combined image of anatomy and trajectories of phase singularities during a certain time period of self-terminated arrhythmia. The phase singularity starts from point A,

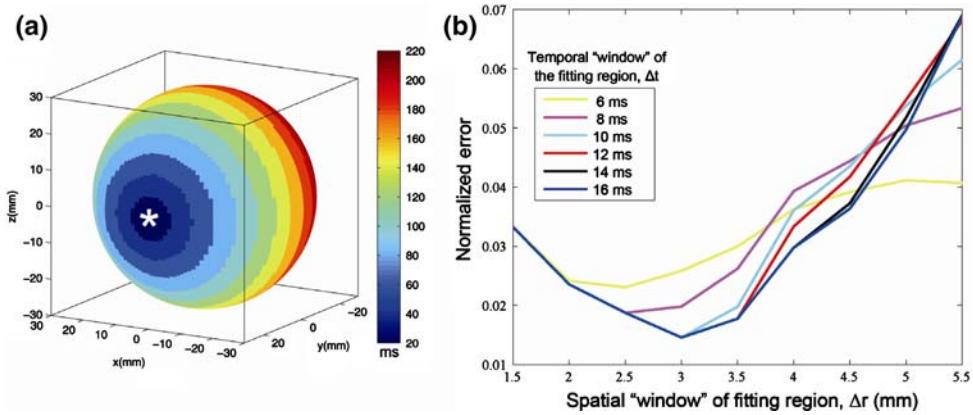

FIGURE 4. Simulation of pacing in a spherical surface. (a) Activation map in the sphere surface by point stimulation at the location noted by an asterisk. The wave propagates radially in a constant speed on the surface. (b) Dependence of the error of conduction velocity on the spatial and temporal "windows" of the fitting region. Suppose one active point, named as center point, is active at Ta. Other active points, which are active at Ti, are included in fitting if their distance from the center point is less than Δr, and $|Ti - Ta| < \Delta t$.

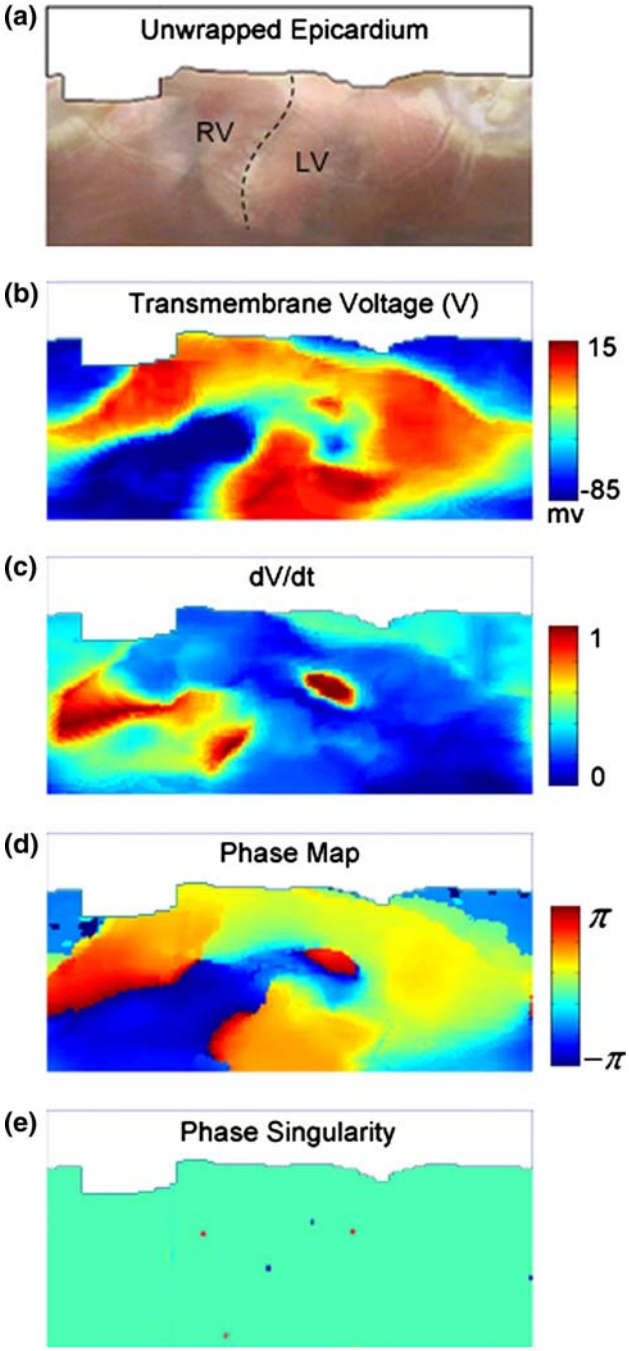

FIGURE 5. Unwrapped presentations. (a) Unwrapped epicardium obtained from digital photographs of the heart. The dashed line represents the septum. (b) Unwrapped epicardial transmembrane voltage (*V*) during ventricular fibrillation. The data is transformed to −85 to 15 mV range from normalized fluorescent signal. (c) Unwrapped *dV/dt* map with value normalized to 0–1. (d) Unwrapped phase map. (e) Phase singularities. Blue dots represent clockwise rotation while red dots represent counterclockwise rotation.

then travels to points B, C, D, and finally hits the AV boundary and terminates. The remaining images of Fig. 7 show the corresponding phase map when the phase singularity is at individual point A, B, C and D. Overall, the ability of global visualization of phase singularities allows the investigation of the nonlinear dynamics of the ventricular arrhythmia, especially when the phase singularity is meandering. Furthermore, the ability to correlate phase singularity with anatomy provides the potentials to investigate the relationship between phase singularity and structural heterogeneities.

Shock-induced VEP is an important mechanism for success and failure of defibrillations.[5–7] Figure 8 shows the VEP induced by far field shock at approximately 85% of APD_{80}. It is already known[6] that shock-induced VEP could generate higher VEP gradient at both base and apex than region in between from anterior view (Fig. 8a), thus creating condition for reentry. With the panoramic setup, not only is the anterior VEP pattern visible, but also the posterior (Fig. 8b). In Fig. 8b, the posterior view shows higher gradient in the base and apex also, similar to what we saw from the anterior. Overall there are four phase singularities created, two in the anterior and two in the posterior. This creates a condition for quatrefoil reentry. Since reentry is unstable in a young normal rabbit heart, the arrhythmia self-terminates after one rotation.

Conduction Velocity in Simulations and Epicardial Pacing

In the simulation, radially propagating waves were constructed on a meshed sphere to mimic epicardial pacing in the heart surface. We optimized the velocity estimation method and tested its validity while changing the size of the spatiotemporal region (the "time window" and "space window") used for polynomial fitting.

We found that estimates of conduction velocity depend weakly on analysis parameters, such as the extents in space and time of the local polynomial fit. Results from simulations with resolution and surface parameters similar to experiment, were used to choose parameters for analysis of experimental data. In the simulation, deviations from exact speed can be tracked. The deviations first decrease, and then increase as the spatial extent of fitting region increases. Figure 4b shows the normalized error of conduction velocity at different spatial and temporal extent of the fitting region. Values for the space and time windows that correspond to the lowest error in simulation were chosen. Note that this non-ideal dependence of velocity estimates on fitting parameters would be reduced if temporal and spatial resolution of activation times were increased significantly. In summary, we found the values of time window and space window that

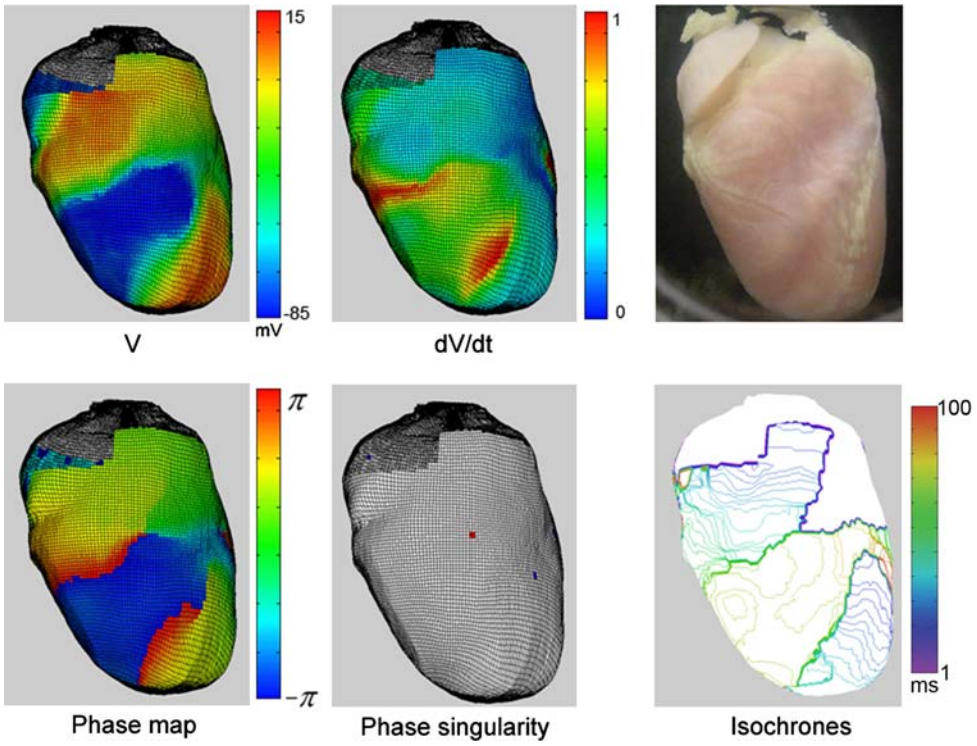

FIGURE 6. Wrapped presentations. Specific notations are present in the figure. The time interval of isochrones is 2 ms.

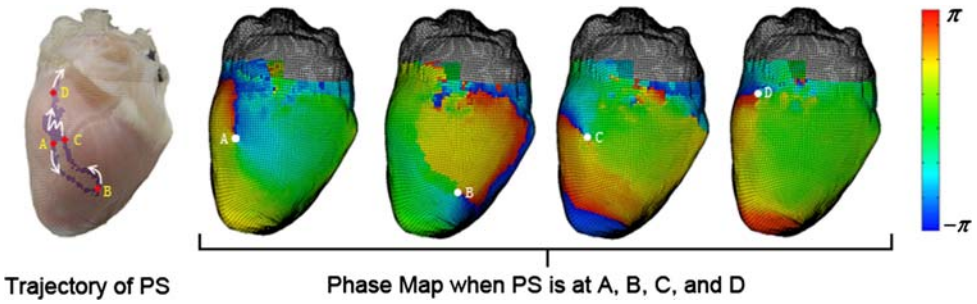

FIGURE 7. Trajectories of phase singularity (PS). The left-most panel is the trajectories of phase singularities on the anatomy. The phase maps corresponding to four phase singularities (A, B, C and D) are also shown.

produced the lowest errors in our simulations, and used them for our experimental data set.

The accuracy of the conduction velocity estimation depends on the polynomial fitting of activation time $t(\theta, \varphi)$. Polynomial fitting eliminates the inaccuracy due to the noise or insufficient resolution by its smoothing effect. This explains why the normalized error initially decreases when the space window increases in Fig. 4b. On the other hand, the error increases when $t(\theta, \varphi)$ is not well fitted. This happens when large space window and/or time window are chosen. This is evident from Fig. 4b that the normalized error starts to increase monotonically as space window becomes larger than certain value.

Figure 9a shows result of application of our method during epicardial pacing. The isochrones and conduction velocity vectors (red arrows) are shown. A snapshot of transmembrane voltage and anatomy are in Fig. 9b. Because of anisotropic conductance, the conduction velocity distribution over various angles has a sinusoidal shape (yellow bars in Fig. 9c). The peak value corresponds to the conduction velocity parallel to fibers; and the minimum value corresponds to the conduction velocity perpendicular to the fiber direction.

Figure 9c also shows the effect of surface curvature on the conduction velocity. If we simplify the calculation by assuming that all signals come from a focal

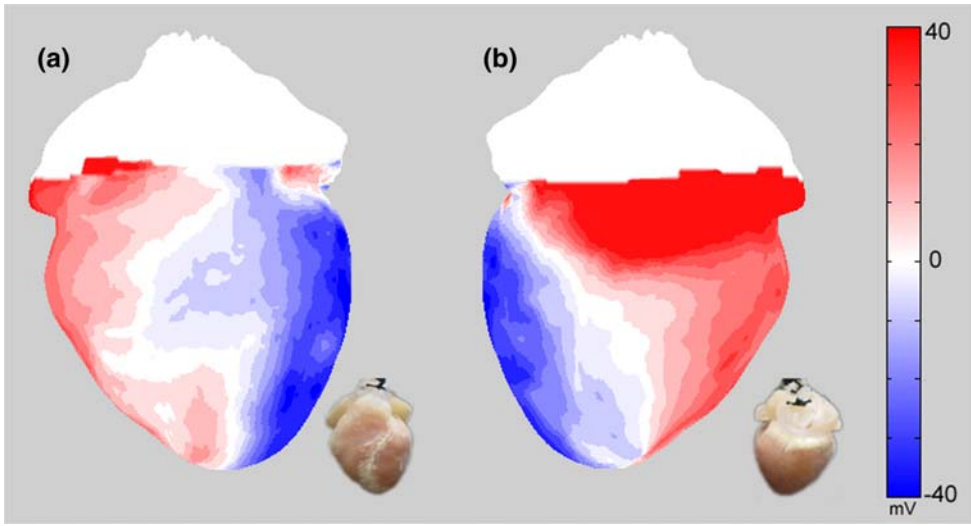

FIGURE 8. Shock-induced virtual electrode (VEP) map. (a) Anterior view. (b) Posterior view.

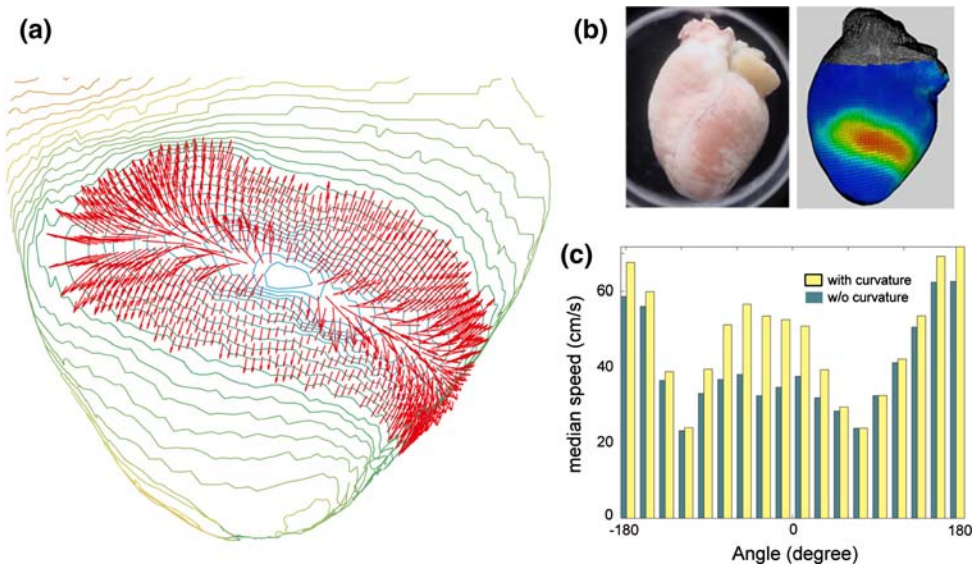

FIGURE 9. Conduction velocity in epicardium during pacing. (a) Conduction velocity vectors after epicardial pacing. The activation isochrones has an interval of 2 ms. (b) Anatomy and snapshot of transmembrane voltage. (c) Conduction velocity versus angles of conduction velocity. The angle of zero corresponds to the direction pointing to right. Angle increases in the counterclockwise manner. The yellow bar represents the condition when curvature of the surface is accounted for during the calculation of conduction velocity, while green bar is the opposite case.

plane, the resultant conduction velocity distribution will be like that in green bars. The green bars are generally shorter than the yellow bar, especially at the peaks. This means that the conduction velocity is underestimated when the velocity component normal to the plane is ignored. Since peak conduction velocity appears more on the edges of the field of view, where surface curves away, the deviations of peak conduction velocity is usually more significant. We quantified the effects of curvature in four hearts on the ratio of conduction velocity along longitudinal and transverse direction. The ratio is 2.45 ± 0.78 when no curvature is considered, different from the ratio 2.98 ± 0.84 when curvature is considered. The ratio is underestimated approximately by 17.8% if the curvature is not considered.

This method can also be applied to reentrant activity during arrhythmia, i.e., ventricular tachycardia, when the conduction is mostly parallel to the epicardium. Figure 10 shows the conduction velocity vectors during stable reentrant spiral waves around a line of block.

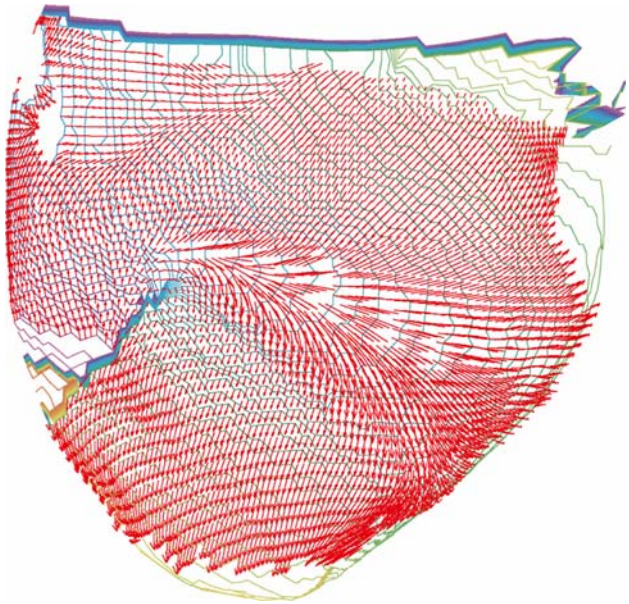

FIGURE 10. Epicardial conduction velocity during reentry. Wave propagates around a line of block which is represented by clustered isochrones. The interval of activation isochrones is 2 ms.

DISCUSSION

In this paper, we presented methods to quantify the panoramic imaging data sets which have not been systematically presented before. We first transformed the mapping data from three PDAs into one 2D array, and then implemented quantitative analysis including dV/dt map, phase map, activation map, and electric stimulus-induced VEP map. We also adapted the method of Bayly *et al.*[1] for conduction velocity to the panoramic data sets. This method is tested on simulated, radially propagating waves on a spherical surface.

Rogers *et al.*[14] introduced another framework for analysis of panoramic data sets by allowing locating phase singularity in an unstructured triangular mesh. This method is more general and works on the complex geometry. Our method, on the other hand, takes advantage of simple geometry of the ventricles and simplicity of grid data set. It is simpler to implement and computationally less expensive.

All the methods mentioned in this paper can be implemented within a reasonable time period during experiment. Once silhouette images are obtained, a low-resolution (e.g., 2 mm) heart surface geometry can be obtained in about 20 s on a Windows PC (Pentium (R) 4, 3.19 GHz CPU, 1.99 GB of RAM) using Matlab 7.0.1 (The Mathworks, Natick, MA). Higher-resolution (e.g., 1 mm) reconstruction takes about 75 s. The user must manually register the heart surface to each PDA field of view, which takes approximately 5–10 min. Then, the heart geometry can be saved and used for texture mapping. This fast and convenient method allows us to reconstruct and analyze every heart mapped in a reasonable amount of time.

The panoramic imaging setup optically mapped almost all the regions of the ventricles and parts of the atria. It should be noted that the spatial resolution at the tip of the apex can be low or almost none since the bottom curves away from every PDA. For the same reason, the spatial resolution is low at the edges of the field of view of every PDA. However, signals generated by these side regions are always simultaneously captured by two PDAs. As a result, sufficient resolution and signal-to-noise ratio can be restored from signals recorded from two PDAs.[13]

Epicardial conduction velocities can be quantified on nearly the entire ventricular epicardium. However, caution needs to be taken to interpret the conduction velocity because conduction is three dimensional in nature. The apparent epicardial conduction velocity is an accurate representation of actual conduction velocity only when the wavefront propagates nearly parallel to the epicardial surface.

The analysis of panoramic mapping data introduced here enhances our ability to investigate the electrophysiology and non-linear dynamics of the heart. This provides an improved global perspective from which to investigate the cardiac conduction in normal and diseased conditions.

REFERENCES

[1]Bayly, P. V., B. H. KenKnight, J. M. Rogers, R. E. Hillsley, R. E. Ideker, and W. M. Smith. Estimation of conduction velocity vector fields from epicardial mapping data. *IEEE Trans. Biomed. Eng.* 45(5):563–571, 1998. doi:10.1109/10.668746.

[2]Bray, M. A., S. F. Lin, and J. P. Wikswo. Three-dimensional surface reconstruction and fluorescent visualization of cardiac activation. *IEEE Trans. Biomed. Eng.* 47(10):1382–1391, 2000. doi:10.1109/10.871412.

[3]Bray, M. A., and J. P. Wikswo. Considerations in phase plane analysis for nonstationary reentrant cardiac behavior. *Phys. Rev. E* 65(5):051902, 2002. doi:10.1103/PhysRevE.65.051902.

[4]Bray, M. A., and J. P. Wikswo. Use of topological charge to determine filament location and dynamics in a numerical model of scroll wave activity. *IEEE Trans. Biomed. Eng.* 49(10):1086–1093, 2002. doi:10.1109/TBME.2002.803516.

[5]Cheng, Y., K. A. Mowrey, D. R. V. Wagoner, P. J. Tchou, and I. R. Efimov. Virtual electrode-induced reexcitation: a mechanism of defibrillation. *Circ. Res.* 85:1056–1066, 1999.

[6]Efimov, I. R., F. Aguel, Y. Cheng, B. Wollenzier, and N. Trayanova. Virtual electrode polarization in the far field: implications for external field. *Am. J. Physiol. Heart Circ. Physiol.* 279:H1055–H1070, 2000.

[7]Efimov, I. R., Y. Cheng, D. R. V. Wagoner, T. Mazgalev, and P. J. Tchou. Virtual electrode-induced phase singularity: a basic mechanism of defibrillation failure. *Circ. Res.* 82:918–925, 1998.

[8]Fedorov, V. V., I. T. Lozinsky, E. A. Sosunov, E. P. Anyukhovsky, M. R. Rosen, C. W. Balke, and I. R. Efimov. Application of blebbistatin as an excitation-contraction uncoupler for electrophysiologic study of rat and rabbit heart. *Heart Rhythm* 4:619–626, 2007. doi:10.1016/j.hrthm.2006.12.047.

[9]Kay, M. W., P. M. Amison, and J. M. Rogers. Three-dimensional surface reconstruction and panoramic optical mapping of large hearts. *IEEE Trans. Biomed. Eng.* 51(7):1219–1229, 2004. doi:10.1109/TBME.2004.827261.

[10]Lin, S. F., and J. P. Wikswo. Panoramic optical imaging of electrical propagation in isolated heart. *J. Biomed. Opt.* 4(2):200–207, 1999. doi:10.1117/1.429910.

[11]Morad, M., and G. Salama. Optical probes of membrane potential in heart muscle. *J. Physiol.* 292:267–295, 1979.

[12]Niem, W. Robust and fast modeling of 3D natural objects from multiple views. *Proc. SPIE* 2182:388–397, 1994. doi:10.1117/12.171088.

[13]Qu, F., C. M. Ripplinger, V. P. Nikolski, C. Grimm, and I. R. Efimov. Three-dimensional panoramic imaging of cardiac arrhythmias in rabbit heart. *J. Biomed. Opt.* 12(4):044019, 2007. doi:10.1117/1.2753748.

[14]Rogers, J. M. Combined phase singularity and wavefront analysis for optical maps of ventricular fibrillation. *IEEE Trans. Biomed. Eng.* 51(1):56–65, 2004. doi:10.1109/TBME.2003.820341.

[15]Rogers, J. M., G. P. Walcott, J. D. Gladden, S. B. Melnick, and M. W. Kay. Panoramic optical mapping reveals continuations epicardial reentry during ventricular fibrillation in the isolated swine heart. *Biophys. J.* 92:1090–1095, 2007. doi:10.1529/biophysj.106.092098.